

UCSF

UC San Francisco Electronic Theses and Dissertations

Title

Dissecting the combinatorial dynamics of NFAT transcription factors during IgE mediated mast cell activation

Permalink

<https://escholarship.org/uc/item/0fg13906>

Author

Takagishi, Seesha

Publication Date

2024

Peer reviewed|Thesis/dissertation

Dissecting the combinatorial dynamics of NFAT transcription factors during IgE-mediated mast cell activation

by
Seesha Takagishi

DISSERTATION
Submitted in partial satisfaction of the requirements for degree of
DOCTOR OF PHILOSOPHY

in

Biochemistry and Molecular Biology

in the

GRADUATE DIVISION
of the
UNIVERSITY OF CALIFORNIA, SAN FRANCISCO

Approved:

DocuSigned by:

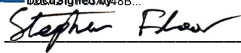
DC0B9413C4A0416... Orion Weiner
Chair

DocuSigned by:

DocuSigned by:2F... Hana El-Samad

DocuSigned by:

DocuSigned by:48B... Vijay Ramani

DocuSigned by:

3709C3C6AF93461... Stephen Floor

Committee Members

Copyright 2024

by

Seesha Takagishi

DEDICATION AND ACKNOWLEDGMENTS

Completing a PhD is extremely challenging, especially given that most of this work was completed during the COVID-19 pandemic. I have many people to thank for helping me along this journey.

First, I thank my advisor, Hana El-Samad. Hana is an incredibly driven and creative scientist with an unbelievable ability to juggle many tasks, insightfully interpret data, and speak to the big picture. She is especially gifted in developing relationships and collaborations with other scientists. She has helped me so much in learning to think about biology from an engineering perspective.

Within the lab, I thank my original rotation mentors Lindsey Osimiri and Alain Bonny, who have incredible dedication to their work while also cultivating a fun lab environment. I thank Matthew Kim, my classmate and labmate, for his humor and willingness to help at any moment. I thank Zara Weinberg for always being willing to talk through experiments, give advice, and for her amazing music taste. Thank you to Sarah Soliman who was always incredibly hard working and generous. Thank you to Hersh for always helping me solve my computational issues and organizing social events. Thank you to the past and present lab managers, Nina Riehs and Manny DeVera, for keeping the lab running so smoothly. Thank you to Melissa and Detzaira for finding time for me to meet with Hana, despite her busy schedule.

Thank you to Tetrad class of 2018, for the laughs and commiseration over shared food. You are all incredibly smart and well-rounded scientists who I look up to a lot. I especially thank Lorenzo Del Castillo, Jocy Lopez, and Haley Gause for help with

reagents and experiments. Thank you also to the Tetrad program coordinators, Toni, Billy, Danny, and Veena for helping guide me through the PhD administrative process.

Thank you to my thesis committee: Orion Weiner, Vijay Ramani, and Stephen Floor, who helped me navigate large scale datasets and negative data to craft a cohesive story.

Thank you to Kari Harrington at the Nikon Imaging Center and Sarah Elmes in the Center for Advanced Technology for their help with core equipment. Thank you to the DNA Technologies Core at UC Davis for their RNA-seq library prep, sequencing, and bioinformatics services.

Thank you to my past advisors Paul Nghiem and Marc Mendillo who supported me in my career advancement, advocated for me, and helped me become an overall better scientist.

I am also fortunate to have been supported by many people outside of UCSF. First, my family, my parents Steve and Colleen Takagishi and my siblings Micah and Kishino Takagishi for supporting me through this extremely challenging process. I would also like to thank my chosen family, particularly Jas Du, Jing Yu, Natalie Lee, Allison Slaughter, Ace Ty, Lorenzo Del Castillo, Megan Chong, Javi Garcia-Bengochoa, my bowling team the Bowlcuts, and the Family Style Collective, I love you all very much, thank you for keeping me sane. Lastly, I would like to give huge thanks to my partner Willy Nicholas for your unfaltering support and love, and especially your help in meeting my nutritional needs.

I thank John Coltrane for the album *A Love Supreme* and the NTS Breakfast Show with Flo Dill for providing the soundtrack for my thesis work. Thank you to Temo's coffee for keeping me caffeinated.

I dedicate this work to the memory of Kumiko (Kay) Takagishi and Fred Yasaki. My grandma Kay went to SF state but was evicted from San Francisco during World War II and incarcerated in Tule Lake at the age of 25. Also at the age of 25, I felt empowered to return to San Francisco on my own accord to start graduate school at UCSF, resisting the forced displacement by replanting my family's roots in the Bay Area. My grandma was a musician and teacher and always encouraged me to seek higher education. Lastly, to Fred, for always making sure I knew I had family here and serving as a link for the rest of the extended family. Our family has a long history of working for the UC system and I feel so fortunate to have been able to attend UCSF as a graduate student. Thank you both for guiding me to San Francisco, I love you both very much, and I hope I've made you proud.

Dissecting the combinatorial dynamics of NFAT transcription factors during IgE
mediated mast cell activation

Seesha Takagishi

ABSTRACT

Although there are many environmental stimuli and possible cellular responses, there are a finite number of transcription factors (TFs) in the cell to coordinate these responses. One way the information carrying capacity of a single signal is multiplexed is through the combinatorial effect of TFs, where two or more inputs modulate the expression of a single gene. Functionally, it has been hypothesized that these combinatorial dynamics are utilized by cells to fine tune cellular responses, such as with the NFAT TFs and the immune response. NFAT (nuclear factor of activated t-cells) activity is regulated both physically and temporally. Physically, NFAT is known to bind several cofactors that modulate the subsequent transcriptional response. Temporally, NFAT isoforms are known to have divergent nuclear translocation responses to the same environmental stimulus. Additionally, a single environmental stimulus could activate several pathways simultaneously, such as the case with NFAT and NFkB, which are both known to behave dynamically. Here, we leverage an epistasis experimental strategy and optogenetics to dissect combinatorial gene regulation involving NFAT1. We replicate the sustained nuclear translocation of NFAT1 and pulsatile nuclear translocation of NFAT4 in response to IgE-mediated mast cell activation in the mast model cell line RBL-2H3. For the first time, we showed that IgE antigen stimulation results in many transcriptional changes, of which only a subset are NFAT1 or NFAT4 specific. We demonstrated that there are distinct and overlapping

roles of NFAT1 and NFAT4 in the IgE antigen transcriptional response, and this response involves other factors. We used the optogenetic tool CLASP (Controllable Light Activated Shuttling and Plasma membrane sequestration) for NFAT1 and successfully controlled NFAT1 nuclear translocation with diverse blue light inputs. We found that blue light alone produced significant transcriptional activity in our cells of interest, but also found that NFAT1-CLASP produced specific NFAT1-like effects upon light-induced translocation. Overall, we identified the NFAT specific signaling downstream of IgE stimulation and demonstrated a system capable of dissecting the information encoded in NFAT1 nuclear translocation dynamics.

TABLE OF CONTENTS

Chapter 1. Introduction	1
Chapter 2. Results	5
NFAT1 and NFAT4 demonstrate distinct nuclear translocation responses to IgE antigen stimulation	5
The transcriptional response to IgE antigen stimulation	8
IgE antigen responsive genes exhibit complicated combinatorial dynamics.....	12
Optogenetic control of NFAT1 nuclear translocation using CLASP	14
The majority of transcriptional effects from blue light stimulation results in off-target gene expression changes	18
NFAT1-CLASP is transcriptionally functional	22
Chapter 3. Discussion	26
Chapter 4. Conclusion.....	28
Chapter 5. Supplementary Figures	29
Chapter 6. Materials and Methods.....	35
Experimental details.....	35
Computational methods	41
Chapter 7. References	44

LIST OF FIGURES

Figure 2.1. IgE-Mediated Mast Cell Activation Results in Distinct NFAT1 and NFAT4 Nuclear Translocation Responses.	7
Figure 2.2. The NFAT1 and NFAT4 Transcriptional Responses to IgE Antigen Stimulation.	10
Figure 2.3. Combinatorial Dynamics of NFAT1 and NFAT4 Target Genes.	13
Figure 2.4. Optogenetic Control of NFAT1 Nuclear Translocation Using CLASP. .	16
Figure 2.5. The Majority of Transcriptional Effects from Blue Light Stimulation Results in Off-Target Gene Expression Changes.	20
Figure 2.6. NFAT1-CLASP is Transcriptionally Functional.	24
Figure 5.1. Supplementary Figure Related to Figure 2.1.	29
Figure 5.2. Supplementary Figure Related to Figure 2.2.	30
Figure 5.3. Supplementary Figure Related to Figure 2.3.	31
Figure 5.4. Supplementary Figure Related to Figure 2.4.	32
Figure 5.5. Supplementary Figure Related to Figure 2.5.	33
Figure 5.6. Supplementary Figure Related to Figure 2.6.	34

LIST OF TABLES

Table 6.1 Plasmids	36
Table 6.2 sgRNA sequences used for CRISPR Cas9 knockout.....	38
Table 6.3 Primers for PCR products used to validate CRISPR Cas9 knockout	38

CHAPTER 1. INTRODUCTION

Transcription factors (TFs) are the master regulators of gene expression in the cell. TFs are responsible for the regulation of many important cellular processes, such as cell fate and apoptosis. There are many layers of regulation that determine the response of a gene to TFs, such as through protein concentration, post-translational modification, and chromatin accessibility. Further, many genes are under combinatorial control, that is, two or more TF inputs can modulate the expression of one gene. Functionally, it has been hypothesized that combinatorial dynamics are utilized by cells to fine tune responses, such as with the NFAT transcription factors and the immune response.¹

The NFAT protein family contains several isoforms that are generally critical for immune cell development and function. The classical NFAT proteins (NFAT1-4) are endogenously regulated by Ca^{2+} -calcineurin signaling.² Under basal conditions, NFAT is highly phosphorylated and resides in the cytosol. Upon high Ca^{2+} levels in the cell, NFAT is dephosphorylated by calcineurin and translocates to the nucleus, subsequently activating downstream gene expression. Interestingly, the NFAT isoforms are activated by distinct calcium signals. NFAT1, for instance, was shown to be activated by a local increase Ca^{2+} levels at microdomains. NFAT4, in contrast, additionally requires nuclear Ca^{2+} levels to rise.³ NFAT4 was also shown to have a more rapid nuclear export rate than NFAT1, which is partly due to the differing SP-3 domains of each isoform.³

NFAT1 is known to bind several cofactors and in some cases the presence of the cofactor dramatically alters the physiological response. For instance, while NFAT1 and AP-1 co-binding increases cytokine and IL-2 production,⁴ when NFAT1 is unable to bind

AP-1 in CD8⁺ T-cells, NFAT1 promotes T-cell anergy and exhaustion.⁵ In contrast, NFAT1 binding to some cofactors has an inhibitory phenotype, such as with Foxp3, which leads to repression of immune genes such as IL-2, IL-4, and IFN- γ .⁴

While many studies of NFAT1 modulation of gene expression focus on the physical interactions between NFAT1 and cofactors, there are also important temporal relationships between TFs. Temporal regulation of NFAT occurs at many levels. For instance, calcium signals themselves occur in pulses and NFAT1 has been shown to integrate calcium load.⁶ Second, TFs within the NFAT protein family demonstrate distinct nuclear patterning in response to the same environmental stimulus. Explicitly, in response to IgE antigen, NFAT1 has slow and sustained accumulation in the nucleus, while NFAT4 pulses in nuclear localization.⁷ Lastly, a single environmental stimulus could activate several signaling pathways simultaneously, leading to several TFs behaving dynamically simultaneously. This is the case of NFAT and NF κ B which each respond with unique patterns of nuclear translocation to environmental inputs.¹

One explanation for these diverse nuclear translocation responses is that dynamic nuclear patterning encodes temporal information, which could be used by the cell to multiplex information about different molecular signals through the same signaling pathway. However, whether gene promoters can respond differentially to different dynamic TF inputs, and how the cell integrates these signals to produce diverse physiological responses, remains poorly understood.

Studying the combinatorial dynamics of TFs using environmental stimuli is difficult because these stimuli often have broad effects on multiple TFs and signaling pathways simultaneously. In contrast, optogenetic tools such as CLASP (Controllable

Light Activated Shuttling and Plasma membrane sequestration) are able to control TF nuclear translocation directly.^{8,9} The use of optogenetics avoids the potential pleiotropic effects of using small molecules to induce TF nuclear translocation, and nuclear import and export occurs rapidly, which allows for replication of natural TF translocation dynamics. For instance, one study of RelA nuclear translocation dynamics found that the use of environmental stimuli can produce transcriptional effects outside of RelA, and RelA-CLASP was used to separate those effects.⁹ TF dynamics can then be interpreted by the cell to produce diverse transcriptional responses, for instance through direct decoding by promoters.¹⁰

NFAT1 is an attractive target for optogenetic control because 1. the use of a blue light stimulus uncouples NFAT1 from the calcium waveform and co-activation of cofactors, and 2. the NFAT1 and NFAT4 nuclear translocation patterns can be shuffled to determine the significance of isoform specific nuclear translocation patterns.

Here, we leverage an epistasis transcriptomics strategy and optogenetics to dissect combinatorial gene regulation involving NFAT1. We replicate the divergent nuclear translocation responses of NFAT1 and NFAT4 in response to IgE mediated mast cell activation. We show that NFAT1 demonstrates sustained localization and NFAT4 exhibits pulsatile nuclear translocation in response to the same stimulus. We conduct an epistasis deletion experiment of NFAT1 and NFAT4 and show that IgE antigen stimulation results in many transcriptional changes, only a subset of which are NFAT1- or NFAT4-specific. Additionally, we demonstrate that IgE antigen responsive genes exhibit complicated combinatorial dynamics. To uncouple the transcriptional changes that are dependent on NFAT alone, we use CLASP to rapidly and reversibly control

nuclear translocation of NFAT1 using blue light. We show that NFAT1-CLASP responds to a variety of both sustained and pulsatile blue light inputs. We also find that blue light stimulation results in CLASP independent transcriptional effects and stratify by stress response to elucidate the specific mechanism of toxicity. In order to mitigate the off-target effects of blue light, we analyze co-differentially expressed genes in NFAT1-CLASP cells treated with blue light and IgE antigen stimulated cells. We show that these genes are enriched for the endogenous NFAT1 binding motif and include known NFAT1 target genes, indicating that NFAT1-CLASP is transcriptionally functional.

CHAPTER 2. RESULTS

NFAT1 and NFAT4 demonstrate distinct nuclear translocation responses to IgE antigen stimulation

NFAT1 and NFAT4 are highly homologous isoforms in the NFAT protein family but NFAT1 and NFAT4 display distinct nuclear translocation responses in response to the same environmental stimuli in the rat basophilic leukemia cell line RBL-2H3, a ubiquitous mast model cell line.⁷ Prior research demonstrated that NFAT1 had a slow and sustained accumulation in the nucleus in response to IgE antigen stimulation, while NFAT4 responded in fast nuclear bursts.⁷ IgE antigen is a natural activator of mast cells that binds to Fcε-receptors on the plasma membrane.¹¹ IgE antigen stimulation also activates NFAT, which in turn mediates the expression of genes involved in the allergy and inflammatory responses.¹²⁻¹⁴

We sought to reproduce these results. We generated cell lines that expressed NFAT1 or NFAT4, fused to mScarlet and an iRFP nuclear marker. We stimulated the cells with two doses of IgE antigen and measured the nuclear translocation patterns of mScarlet tagged NFAT1 and NFAT4 using live cell imaging. We found that NFAT1 demonstrated a slow and continuous accumulation in the nucleus (Figure 2.1 A,B). In contrast, NFAT4 pulsed in nuclear localization in response to IgE antigen (Figure 2.1C, Figure 5.1G). The duration of bursts increased in response to IgE antigen dose (7.9, 12.1 minute bursts for low and high IgE antigen, $p = 0.007$) (Figure 2.1D). The average number of bursts did not significantly change with IgE antigen dose (2.6, 2.06 for low and high IgE antigen, $p = 0.30$) (Figure 2.1E).

The average nuclear import time for NFAT1 was 5.0 and 3.2 minutes for low and high IgE antigen doses, respectively (Figure 5.1E). The average nuclear import time for NFAT4 was similar to NFAT1 at 6.5 and 4.4 minutes for low and high IgE antigen doses (Figure 5.1F).

The dynamic nuclear translocation patterns of NFAT1 and NFAT4 encode temporal information, which could be used by the cell to multiplex information about different molecular signals through the same signaling pathway. Given this hypothesis, we then asked whether the cell can decode these signals to produce diverse physiological responses (Figure 2.1F).

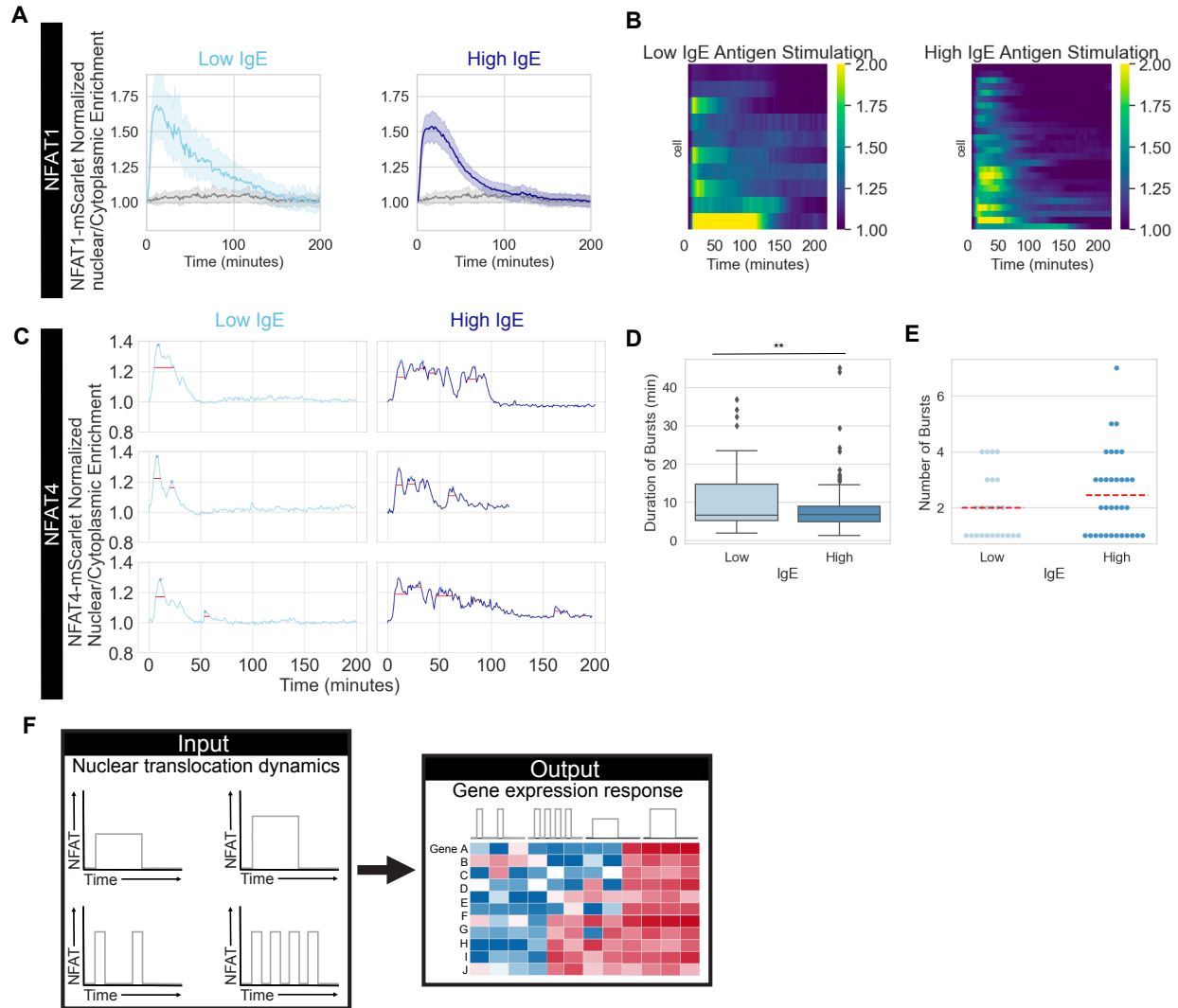


Figure 2.1. IgE-Mediated Mast Cell Activation Results in Distinct NFAT1 and NFAT4 Nuclear Translocation Responses. (A) Average cell trace of nuclear/cytoplasmic enrichment of NFAT1-mScarlet over time for a low dose (left) or high dose (right) of IgE antigen. The average cell trace for no treatment is displayed in gray. (B) Heatmap of nuclear/cytoplasmic enrichment of NFAT1-mScarlet over time for each individual cell. (C) Representative single cell traces of NFAT4-mScarlet for low doses (left) or high doses (right) of IgE antigen. (D) Duration of NFAT4 nuclear bursts in response to low and high IgE antigen. The mean value is represented by the red dotted line. (E) Number of NFAT4 nuclear bursts in response to low and high IgE antigen. The mean value is represented by the red dotted line. (F) Schematic hypothesis of how differing nuclear translocation dynamics may produce diverse gene expression responses.

The transcriptional response to IgE antigen stimulation

In order to perform an epistasis deletion experiment, we generated clonal CRISPR-Cas9 mediated knockouts of NFAT1 and NFAT4 (Δ NFAT1 and Δ NFAT4). We used a scramble sgRNA as a non-targeting control (sgNT). We verified the knockout through NGS and a computational analysis (Figure 5.2A,B, also see Computational Methods *CRISPR clone generation*). We pre stimulated knockout and control cells overnight with anti-TNP IgE antibodies to cluster IgE-Fc ϵ r1 receptors. We then activated the receptors with TNP-BSA at time 0, and harvested at two separate time points. (Figure 2.2A)

A principal component analysis revealed that samples primarily clustered by cell type, and secondarily by time point (Figure 2.2B,C). In the sgNT cell line, we found the number of DEGs at the early time point versus the late time point were similar (50min vs 100min: High IgE, 313 vs 321 DEGs, Low IgE, 381 vs 338 DEG's) (Figure 2.2D). However, there were a larger number of DEGs with a log fold change >1 at the early time point (50min vs 100min: High IgE, 96 vs 50 DEGs, Low IgE, 108 vs 45 DEGs).

The early transcriptional changes were enriched for TNF α signaling via NF κ B, response to wounding, and regulation of multicellular organismal development (Cluster 2, Figure 2.2E). Highly upregulated genes at both time points were additionally enriched for NGF-stimulated transcription, the SRF motif, and nuclear events (kinase and transcriptional factor activation) (Cluster 4, Figure 2.2E). Moderately upregulated genes were enriched for TNF α signaling via NF κ B, negative regulation of multicellular organismal process, the AP4 motif, negative regulation of signaling, and positive regulation of programmed cell death (Cluster 3, Figure 2.2E).

We next determined significantly differentially expressed genes in IgE antigen treated cells versus no treatment in the Δ NFAT1 and Δ NFAT4 cell lines. We compared these lists of DEGs to those significantly differentially expressed in the sgNT cell line. We found that 477 (61%) of genes were differentially expressed only in sgNT and not Δ NFAT1 (NFAT1 specific), and 552 (71%) differentially expressed only in sgNT and not in Δ NFAT4 (NFAT4 specific) (Figure 2.2F,G). We found that most of the NFAT1 and NFAT4 specific genes are co-regulated by NFAT1 and NFAT4 (NFAT1 specific: 408/552(74%), NFAT4 specific: 408/477(86%), Figure 2.2H).

Next, we asked how the dynamics of these genes were modulated by NFAT1 and NFAT4.

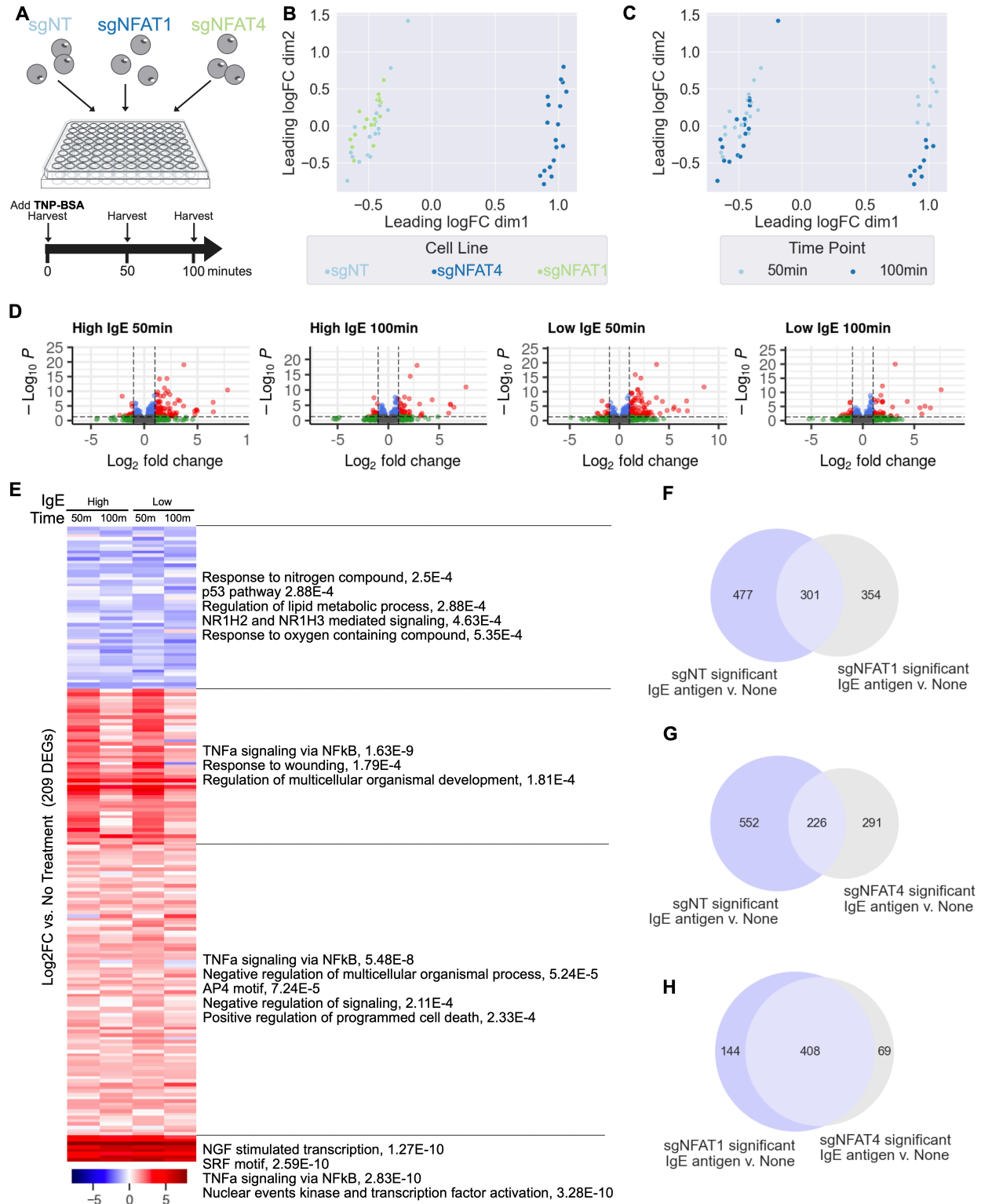


Figure 2.2. The NFAT1 and NFAT4 Transcriptional Responses to IgE Antigen Stimulation. (A) Experimental design of RNA-Seq experiment. (Figure caption continued on the next page.)

(Figure caption continued from the previous page.) Three different cell lines were individually plated and stimulated with IgE antigen and TNP-BSA. Cells were harvested at 0, 50, and 100 minutes. (sgNT = Non-Targeting sgRNA) (B) PCA plot of RNA-Seq data stratified by cell line. (C) PCA plot of RNA-Seq data stratified by time point. (D) Volcano plots examining the difference between IgE antigen stimulation and no treatment in the sgNT cell line, separated by IgE antigen dose (low, high) and time (50, 100min). (E) Heatmap of the union of significantly differentially expressed genes comparing IgE antigen stimulation to no treatment in the sgNT cell line. There were a total of 209 DEGs. This heatmap was k-means clustered into 4 distinct clusters. (F) Venn diagram comparing the union of significantly differentially expressed genes in IgE antigen stimulation versus no treatment in the sgNT cell line, versus the sgNFAT1 cell line. (G) Venn diagram comparing the union of significantly differentially expressed genes in IgE antigen stimulation versus no treatment in the sgNT cell line, versus the sgNFAT4 cell line. (H) Venn diagram comparing the union of significantly differentially expressed genes in IgE antigen stimulation versus no treatment in the sgNFAT1 cell line, versus the sgNFAT4 cell line.

IgE antigen responsive genes exhibit complicated combinatorial dynamics

We took the genes that were responsive to IgE antigen stimulation in the sgNT cells, and used hierarchical clustering to identify clusters of genes with different dynamic profiles between sgNT and Δ NFAT1 or Δ NFAT4. 11 clusters of genes were identified comparing sgNT and Δ NFAT1 in the high IgE antigen treatment group, and 12 clusters in the low IgE antigen treatment group (Figure 2.3A, Figure 5.3A). The majority of genes exhibited decreased responsiveness in the Δ NFAT1 cells, while a subset of genes also had an increased effect or were unresponsive in the Δ NFAT1 cells (Figure 2.3C).

Similarly, there were 13 clusters of genes identified when comparing sgNT and Δ NFAT4 cells treated with high IgE antigen, and 12 clusters in the cells treated with low IgE antigen (Figure 2.3B, Figure 5.3B). The majority of genes also exhibited a decreased effect in Δ NFAT4 compared to sgNT, while a subset of genes also displayed an increased effect in the Δ NFAT4 cells or were unresponsive (Figure 2.3D). Interestingly, there were a large number of genes with increased expression in the Δ NFAT4 cells treated with a high dose of IgE antigen stimulation (28%, Figure 2.3D).

Further, several genes exhibited clear patterns in both doses of IgE antigen (Figure 2.3E,F). We next asked which genes were responsive to nuclear translocation of NFAT1 alone.

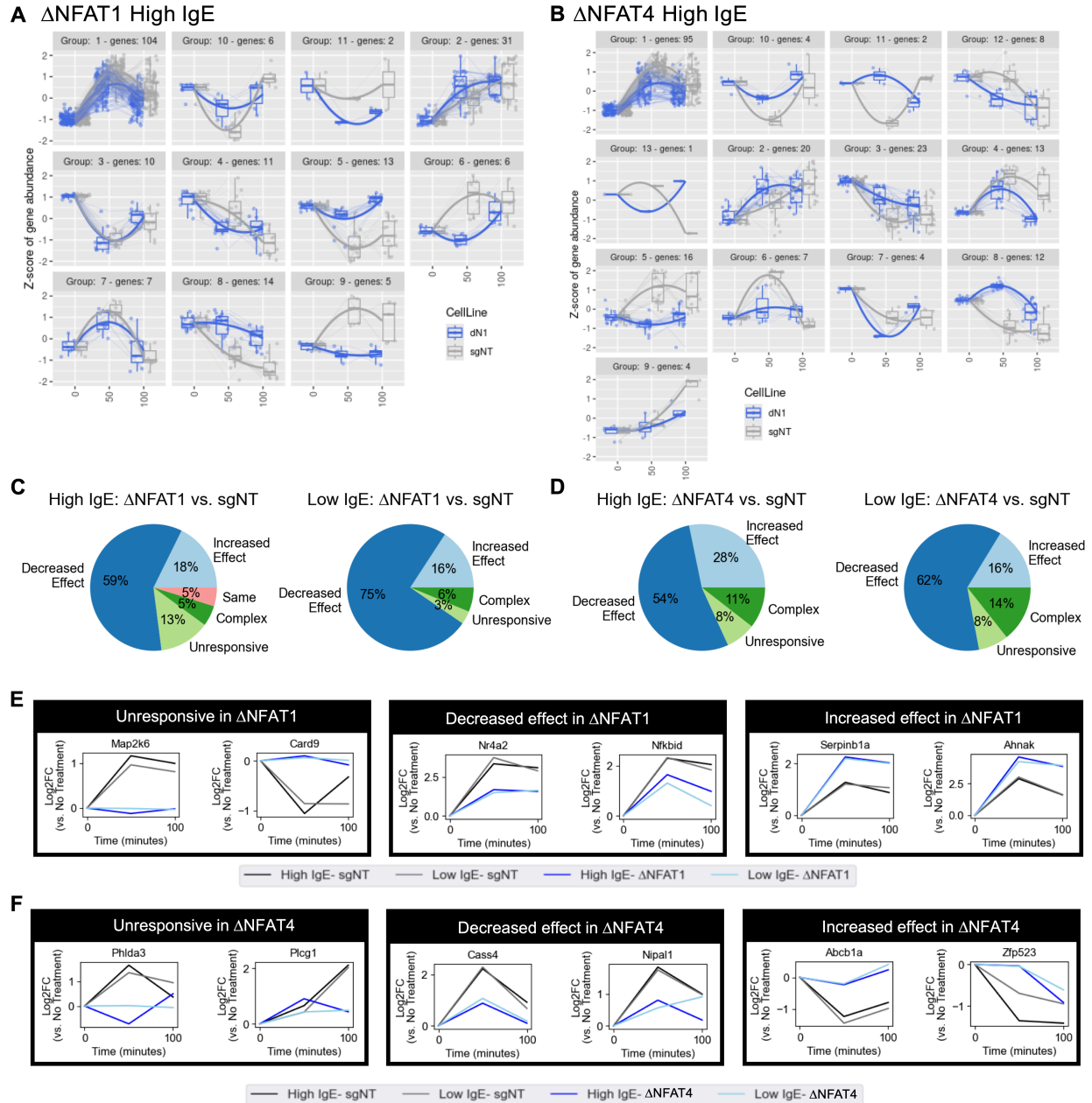


Figure 2.3. Combinatorial Dynamics of NFAT1 and NFAT4 Target Genes. (A) IgE antigen responsive genes clustered by gene patterns in sgNT (grey) and dN1 (blue). sgNT = Non-Targeting sgRNA. dN1 = Δ NFAT1. (B) IgE antigen responsive genes clustered by gene patterns in sgNT (grey) and dN4 (blue). sgNT = Non-Targeting sgRNA. dN4 = Δ NFAT4. (C) Characterization of gene clusters from A, represented as proportion of the total. (D) Characterization of gene clusters from B, represented as proportion of the total. (E) Representative genes from the clusters in A. F. Representative genes from the clusters in B.

Optogenetic control of NFAT1 nuclear translocation using CLASP

One disadvantage of using natural inputs to induce nuclear translocation is that the transcriptional response may involve other factors. To provide a cleaner input, we adapted the optogenetic tool CLASP (Controllable Light Activated Shuttling and Plasma membrane sequestration), originally developed in *S. Cerevisiae*, for the rat basophilic leukemia cell line RBL-2H3.

CLASP utilizes two asLOV2 domains, blue light-sensitive proteins derived from *Avena sativa*, to sequester protein cargo at the plasma membrane in the dark. In response to blue light, the asLOV2 domains release the cargo and expose a nuclear localization signal (Figure 2.4A). We utilized a constitutively nuclear mutant of NFAT1 to break the endogenous control of nuclear translocation (Figure 5.4A). We show that NFAT1-CLASP had minimal basal localization in the dark (Figure 2.4C). NFAT1-CLASP rapidly translocated to the nucleus using as little as 449au of blue light, and quickly exited the nucleus in the dark (Figure 2.4B-D). Thus, NFAT1-CLASP demonstrated rapid and reversible control of nuclear translocation using blue light.

Next, we asked whether we were able to mimic the nuclear translocation patterns of NFAT1 and NFAT4 using blue light. Indeed, we found that constitutive blue light led to sustained NFAT1-CLASP nuclear localization (Figure 2.4C). We also found that delivering different regimes of pulsed light to NFAT1-CLASP expressing cells was effective in replicating NFAT4 translocation responses to IgE antigen stimulation. NFAT1-CLASP responded to blue light pulses as rapid as 5min ON/10m OFF, and 5m ON/5m OFF (Figure 2.4C). We found that the normalized nuclear/cytoplasmic enrichment did not significantly change with light intensity (Figure 2.4E).

NFAT1 translocated to the nucleus on average between 5.9 to 9.8 minutes after blue light exposure for each light intensity (Figure 2.4F). This was comparable to the nuclear import rate of NFAT1-GFP (3.2 and 5 minutes on average for low and high IgE) and NFAT4-GFP (4.4 and 6.5 minutes on average for low and high IgE) in response to IgE antigen stimulation (Figure 5.1E,F). Nuclear export was calculated after the blue light was turned off. We found that NFAT1 exited the nucleus on average between 4.4 to 6.5 minutes for different light intensities (Figure 2.4G).

Next, we asked whether we were able to replicate the NFAT1 transcriptional response to IgE antigen using blue light (Figure 2.4H). A secondary question was whether we were able to reprogram the transcriptional response of NFAT1 by shuffling the nuclear translocation patterns of NFAT1 and NFAT4 using blue light (Figure 2.4H).

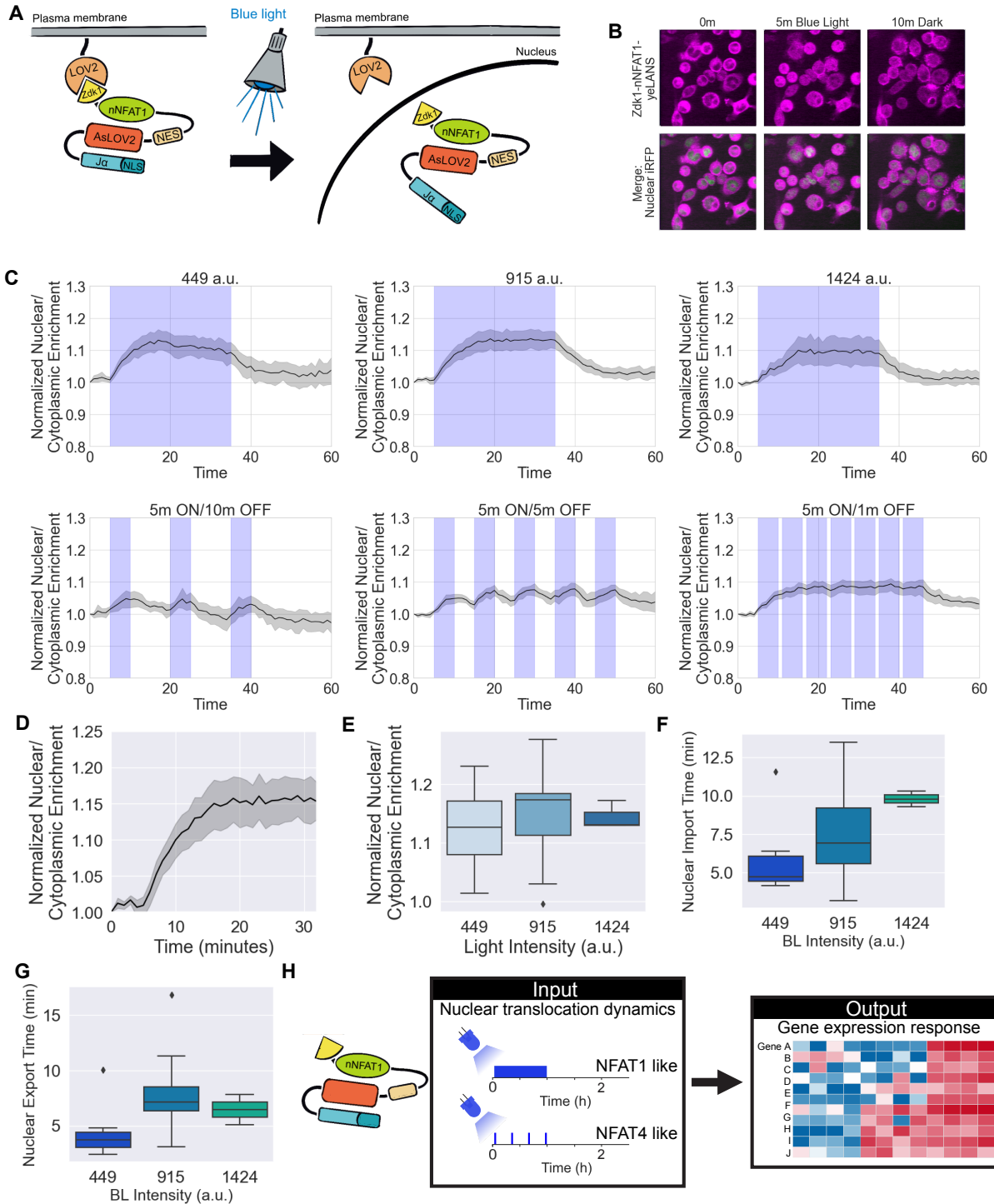


Figure 2.4. Optogenetic Control of NFAT1 Nuclear Translocation Using CLASP. (A) Schematic of the function of CLASP. (B) Representative images of nNFAT1-CLASP cells in response to blue light (915au). (C) nNFAT1-CLASP normalized nuclear/cytoplasmic enrichment over time for sustained (top) and pulsatile (bottom) blue light inputs. (D) Nuclear import of nNFAT1-CLASP in response to 915 a.u. of blue light. (Figure caption continued on the next page.)

(Figure caption continued from the previous page.) (E) Comparison of the maximum nuclear/cytoplasmic enrichment versus light input intensity. F. Nuclear import time of nNFAT1-CLASP stratified by blue light intensity, calculated between 5 and 25 minutes. G. Nuclear export time of nNFAT1-CLASP stratified by blue light intensity, calculated between 35 and 55 minutes. H. Experimental strategy of utilizing pulsatile and sustained light inputs on nNFAT1-CLASP cells to determine the resulting transcriptional responses.

The majority of transcriptional effects from blue light stimulation results in off-target gene expression changes

To minimize blue light toxicity for extended durations of blue light, we delivered rapid pulses of blue light (2s ON/2s OFF), fast enough that NFAT1 cargo did not leave the nucleus (Figure 5.5A). We showed that this regime did not have significant toxicity relative to blue light in cells expressing the full NFAT1-CLASP tool or membrane-tethered LOV2 alone (“trap only”), even in blue light regimes for up to two hours at the maximum blue light dose (Figure 5.5B).

Four blue light waveforms were used: 915 a.u. sustained light, 1424 a.u. sustained light, 10m ON/50m OFF pulsatile light, and 10m ON/20m OFF pulsatile light. RNA was harvested at 0.5, 1, and 2 hours. We controlled for the effect of blue light on transcription by stimulating “trap only” cells as a control (Figure 2.5A).

A principal component analysis revealed the primary source of variation between samples was the duration of blue light exposure (Figure 2.5B). Indeed, we found that 3100 genes were significantly differentially expressed in the Trap only cell line when comparing sustained light versus no light, and 1347 of these genes had a log fold change > 1 compared to no light (Figure 2.5B).

To narrow in on the specific stress responses the blue light was triggering, we calculated the enrichment of common stress signatures with the list of genes significantly differentially expressed in the Trap only cell line. In particular, we found that DNA repair, cellular response to heat stress, and UV response gene signatures were enriched (Figure 2.5D).

Only 254/1269 (20%) of genes were significantly differentially expressed in the NFAT1-CLASP cell line and not the Trap only cell line when comparing sustained light versus no light (Figure 5.5D). Given the extreme transcriptional effect of blue light, we tested whether there were additional phenotypes outside of cellular viability that were impacted by blue light. We found that cellular proliferation was slightly shifted in comparison to the no light control in the Trap only cell line (Figure 2.5E).

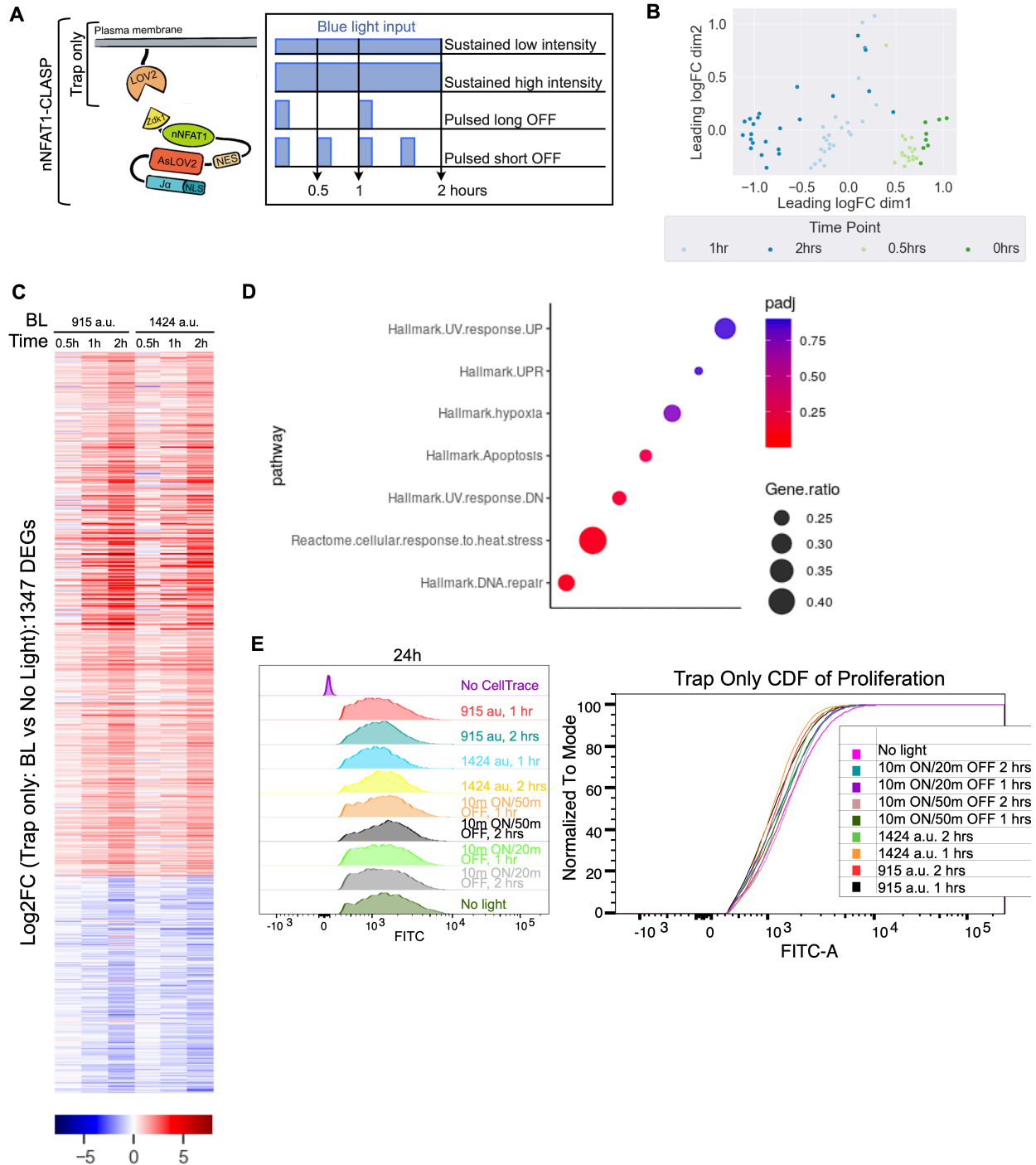


Figure 2.5. The Majority of Transcriptional Effects from Blue Light Stimulation Results in Off-Target Gene Expression Changes. (A) Experimental design of RNA-Seq experiment. Two cell lines were used: nNFAT1-CLASP and Trap only. Four different patterns of blue light inputs were used. Cells were harvested at 0.5, 1, and 2 hours. (B) PCA plot of nNFAT1-CLASP RNA-Seq data stratified by time point. (C) Heatmap representing the union of significantly differentially expressed genes in the Trap only cell line exposed to sustained light inputs. Heatmap includes 1347 DEGs. Data was k-means clustered into 2 clusters. (Figure caption continued on the next page.)

(Figure caption continued from the previous page.) (D) Dot plot of enriched stress response motifs for the genes shown in (C). (E) Flow data of FITC expression in cells incubated with CellTrace following blue light stimulation (left) and the cumulative distribution function (right) of this flow data.

NFAT1-CLASP is transcriptionally functional

We filtered the significantly differentially expressed genes in the NFAT1-CLASP cell line exposed to sustained blue light by the genes that were significantly differentially expressed in the Trap only cell line, leaving 254 genes (20%, Figure 2.6A). To increase confidence that these were on-target genes for NFAT1, we compared this list to genes that were differentially expressed in response to IgE antigen stimulation in sgNT cells, and in the Δ NFAT1 cell line.

We found that 35/254 genes (14%) were co-differentially expressed between NFAT1-CLASP exposed to sustained blue light and sgNT stimulated with IgE antigen (Figure 2.6B). Of these genes, 21/35 (60%) were determined to be NFAT1 specific (Figure 2.6B).

The 35 common genes between IgE antigen stimulation in sgNT cells and NFAT1-CLASP specific sustained light included both upregulated and downregulated genes (Figure 2.6C).

We noted that several of the 35 common genes are involved in biological processes canonically associated with NFAT1, such as lymphocyte activation (Ripk2, Nfkbiz, Bad, Swap70, Themis2, Hsh2d) and the inflammatory response (Ripk2, Nfkbiz, Csf1, Ptgs2, Themis2, Abcf1). These common genes also included genes that are implicated in cell death (Ubxn2a) and genes involved in the osmotic stress response (Bad, Ptgs2).¹⁵ We note that genes are both positive and negatively regulated by NFAT1 in a CLASP dependent manner (Figure 2.6D). Lastly, we completed a motif analysis of these 35 DEG's. Two motifs for NFATc2 (NFAT1) were enriched (Figure 2.6E).

We next investigated the 40 genes that were co-differentially expressed between NFAT1-CLASP exposed to pulsatile blue light and sgNT stimulated with IgE antigen (Figure 2.4G). Included in this list were genes associated with the regulation of autophagy (Usp13, Phf23, Ripk2, Sesn3, Srebf1, Atf6), IL2 STAT5 signaling (Ndr1, Map3k8, Swap70, Slc39A8), and cell activation (Egr1, Ndr1, Cd151) (Figure 2.5H). The top 5 enriched motifs for this set of genes were Ezh2, Irf8, Irf3, E2F6, and Foxo1. Interestingly, none of the NFAT binding motifs were enriched.

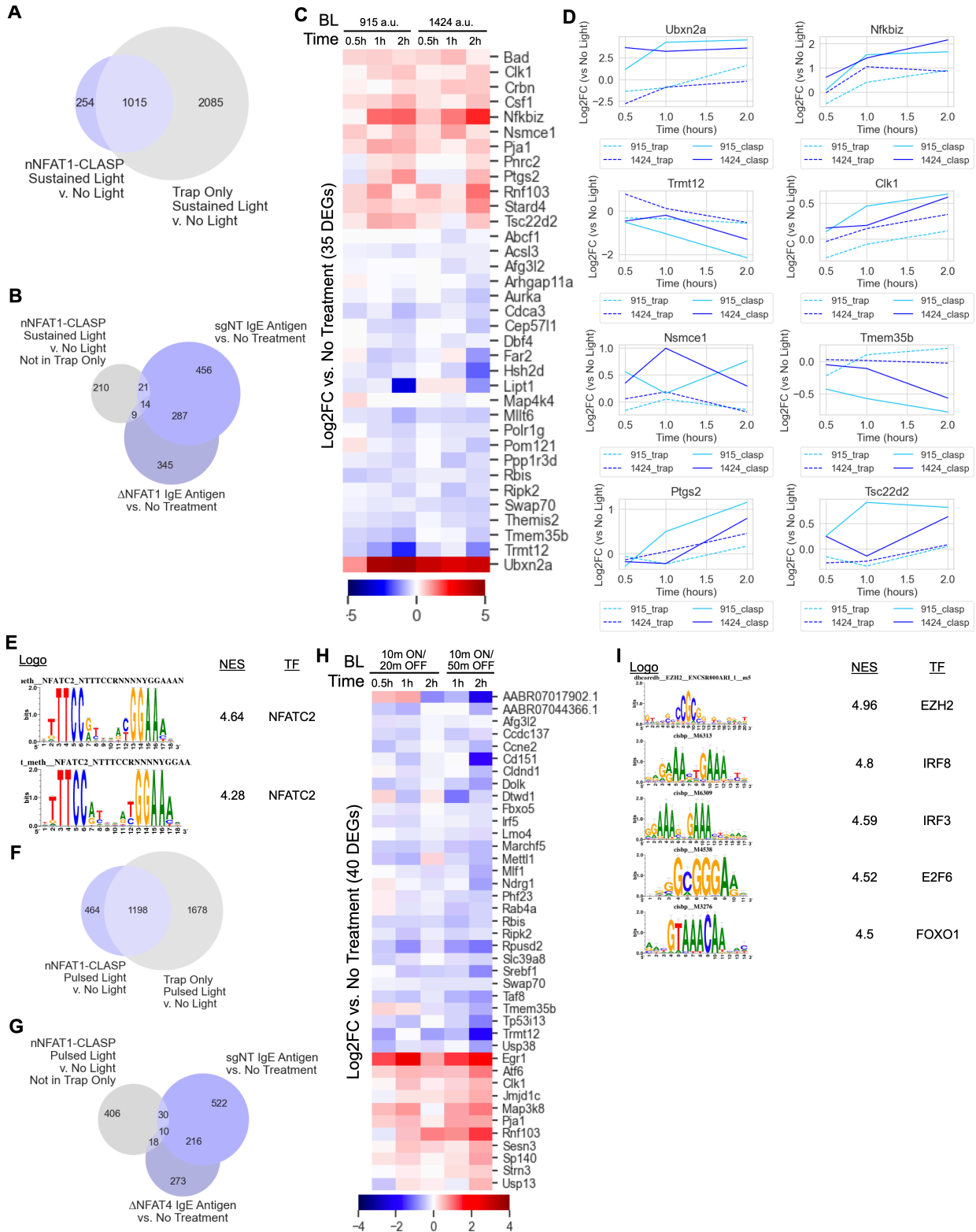


Figure 2.6. NFAT1-CLASP is Transcriptionally Functional. (Figure caption continued on the next page.)

(Figure caption continued from the previous page.) (A) Venn diagram comparing the union of significantly differentially expressed genes between nNFAT1-CLASP and Trap only cells stimulated with sustained blue light. (B) Triple venn diagram comparing the union of significantly differentially expressed genes in nNFAT1-CLASP and not Trap only cells stimulated with sustained blue light, IgE antigen versus no treatment in the sgNT cell line, and IgE antigen versus no treatment in the sgNFAT1 cell line. (C) Heatmap of common significantly differentially expressed genes (35 DEGs) between nNFAT1-CLASP and not Trap only cells stimulated with sustained blue light and IgE antigen versus no treatment in the sgNT cell line. Rows are annotated with the gene name. (D) Specific genes from the heatmap in (C), plotted as the Log₂FC (Light versus No Light) versus time. The solid lines represent the nNFAT1-CLASP cell line and the dotted lines represent the Trap only cell line. (E) Enriched NFAT motifs from the genes from the heatmap in (C). (F) Venn diagram comparing the union of significantly differentially expressed genes between nNFAT1-CLASP and Trap only cells stimulated with pulsatile blue light. (G) Triple venn diagram comparing the union of significantly differentially expressed genes in nNFAT1-CLASP and not Trap only cells stimulated with pulsed blue light, IgE antigen versus no treatment in the sgNT cell line, and IgE antigen versus no treatment in the sgNFAT4 cell line. (H) Heatmap of common significantly differentially expressed genes (40 DEGs) between nNFAT1-CLASP and not Trap only cells stimulated with pulsatile blue light and IgE antigen versus no treatment in the sgNT cell line. Rows are annotated with the gene name. (I) Top 5 enriched binding motifs from the genes in (H).

CHAPTER 3. DISCUSSION

It is known that NFAT1 and NFAT4 display distinct translocation dynamics, however, here we showed for the first time how these translocation dynamics impacted transcription. We elucidated the differential and combinatorial effects of NFAT1 and NFAT4 on gene expression. These analyses illustrate the complexity of mast cell activation, involving overlapping and distinct roles of NFAT1, NFAT4, and additional factors.

Many genes were co-differentially expressed between non-targeting and knockout cell lines in response to IgE antigen stimulation, which we hypothesize are the result of co-factor binding or redundancy. In fact, the majority of genes that were responsive to IgE antigen stimulation in the non-targeting cells demonstrated reduced Log₂FC in the knockout cells. However, these genes were not completely unresponsive. This indicates that there are additional molecular players modulating the expression of these genes. Interestingly, a significant portion of genes also displayed an increased effect in Δ NFAT1 and Δ NFAT4 cells compared to the non-targeting cells. This indicates that there is perhaps a repressor working with NFAT1 and NFAT4 to suppress gene expression. Further experiments are needed, however, to determine whether this relationship is direct or indirect.

We also found that blue light could be used to recapitulate the nuclear translocation responses of both NFAT1 and NFAT4 to IgE antigen stimulation, using the optogenetic tool NFAT1-CLASP. However, we found that although blue light did not substantially affect cell viability, cellular proliferation was moderately affected, and extreme transcriptional effects were observed. Optogenetics is becoming common and

off target effects have been demonstrated in other studies as well. Additionally, this could be a non-cell autonomous interaction, such as a species generated from media.¹⁶ In order to circumvent these issues, additional studies could focus on decreasing blue light intensity, mutating LOV2 in order to reduce the blue light required for translocation, or including additional replicates to increase statistical power and therefore confidence in on-target genes.

Despite the blue light toxicity, our preliminary results indicate that NFAT1-CLASP is transcriptionally active. We note that the translocation of NFAT1 alone is sufficient to modulate the expression of a subset of NFAT1 target genes. However, the reprogramming of NFAT1 with the NFAT4 nuclear translocation pattern did not lead to enrichment of NFAT4 binding motif.

Further, there were 23 genes present in both the NFAT1-CLASP and Δ NFAT1 IgE treated cells, which suggests that these genes can be regulated by NFAT1 but could also be regulated otherwise. Interestingly, 12 of these 23 genes were regulated in different directions between NFAT1-CLASP and IgE antigen treated Δ NFAT1 cells, indicating that the additional factors which affect this subset of genes work in opposition to NFAT1 (Figure 5.6E). However, the FDR values for this preliminary experiment are not convincing, and so these experiments should be repeated in a context with less blue light toxicity. Further studies are required to make conclusions about specific sets of genes that are affected by NFAT1 translocation alone using NFAT1-CLASP.

CHAPTER 4. CONCLUSION

Dissecting the combinatorial effects of NFAT1 and NFAT4 on transcription is a challenge because these transcription factors bind to the same DNA sequences and their activity is modulated by a variety of co-factors. Here, we demonstrated that we could investigate these combinatorial dynamics using a combination of optogenetics, transcriptomics, and epistasis experiments using natural inputs. Despite having differing nuclear translocation dynamics, NFAT1 and NFAT4 have overlapping gene regulons. Many of the NFAT1 and NFAT4 target genes' expression was not eliminated by NFAT1 or NFAT4 deletion, which provided evidence of regulation by additional factors. We also conducted a proof-of-concept experiment with the optogenetic tool NFAT1-CLASP and showed that NFAT1 translocation alone is sufficient to activate a subset of NFAT1 target genes. We also found that despite many studies using cell survival alone to determine optimal blue light doses, blue light may surreptitiously impact cell proliferation over time and activate stress responses such as the UV damage response and the heat shock response. Further experiments are required to determine the specific mechanism of blue light toxicity. Through reducing blue light doses or increasing replicates, higher confidence gene targets could be determined, therefore providing a basis to investigate decoding of nuclear translocation dynamics by promoters and enhancers. This system could be multiplexed with additional optogenetic tools activated with different light waveforms to determine the effect of NFAT1 and NFAT4 translocation simultaneously. NFAT1-CLASP could also be used in conjunction with natural inputs in the deletion cell lines to determine the impact of coactivation of additional factors on gene expression.

CHAPTER 5. SUPPLEMENTARY FIGURES

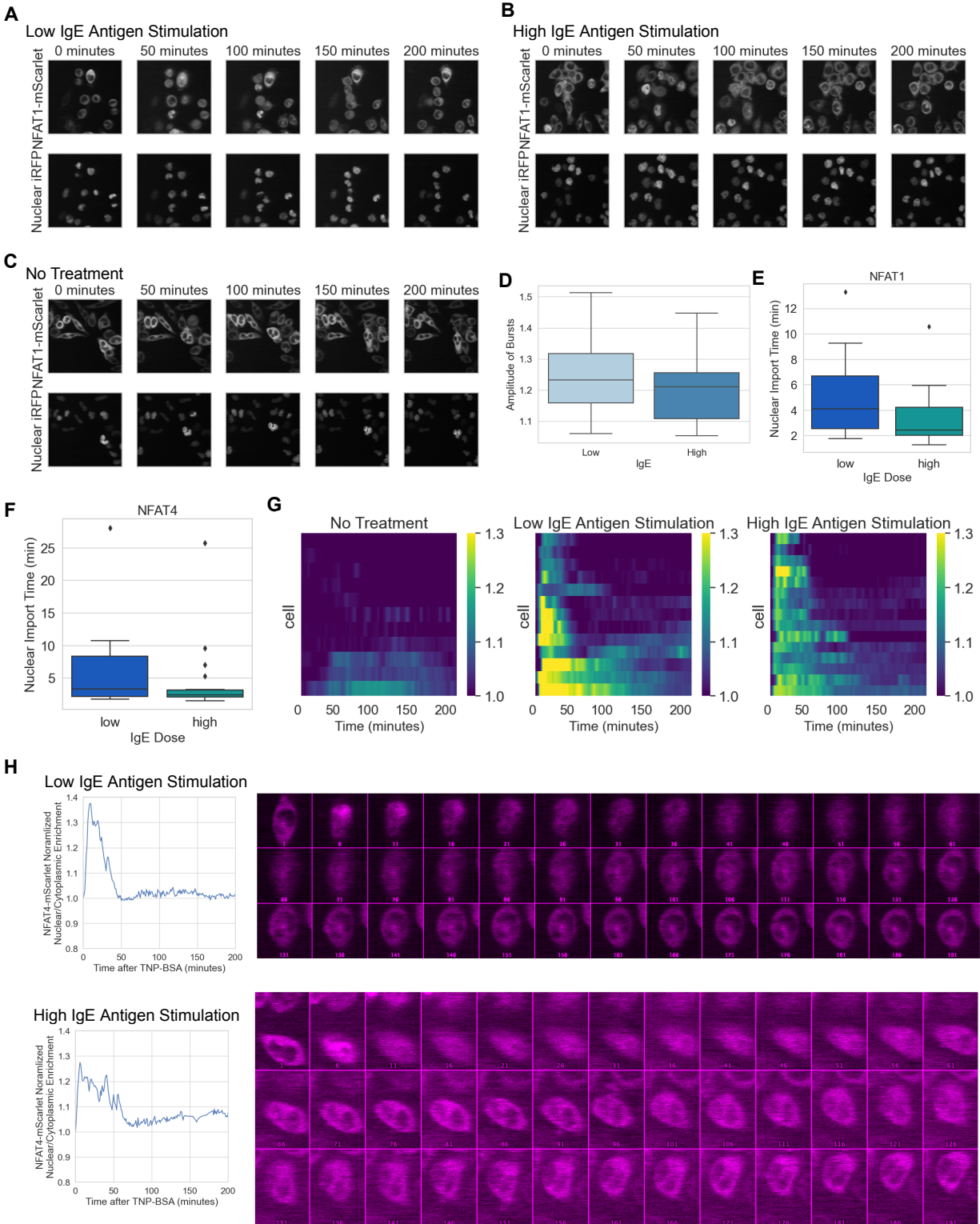


Figure 5.1. Supplementary Figure Related to Figure 2.1. (Figure caption continued on the next page.)

(Figure caption continued from the previous page.) (A) Images of NFAT1-mScarlet nuclear localization over time, stimulated with a low dose of IgE antigen. (B) Images of NFAT1-mScarlet nuclear localization over time, stimulated with a high dose of IgE antigen. (C) Images of NFAT1-mScarlet nuclear localization over time, with no treatment. (D) Amplitude of NFAT4-mScarlet bursts for each individual cell, stratified by dose of IgE antigen. (E) Nuclear import time of NFAT1-mScarlet stratified by IgE antigen dose, calculated between 0 and 20 minutes for low IgE antigen and 0 and 42 minutes for high IgE antigen. (F) Nuclear import time for NFAT4-mScarlet stratified by IgE antigen dose, calculated between 0 and 15 minutes for low IgE antigen and 0 and 17 minutes for high IgE antigen. (G) Single cell trace and corresponding images for a representative NFAT4-mScarlet cell stimulated with low IgE antigen. (H) Single cell trace and corresponding images for a representative NFAT4-mScarlet cell stimulated with high IgE antigen.

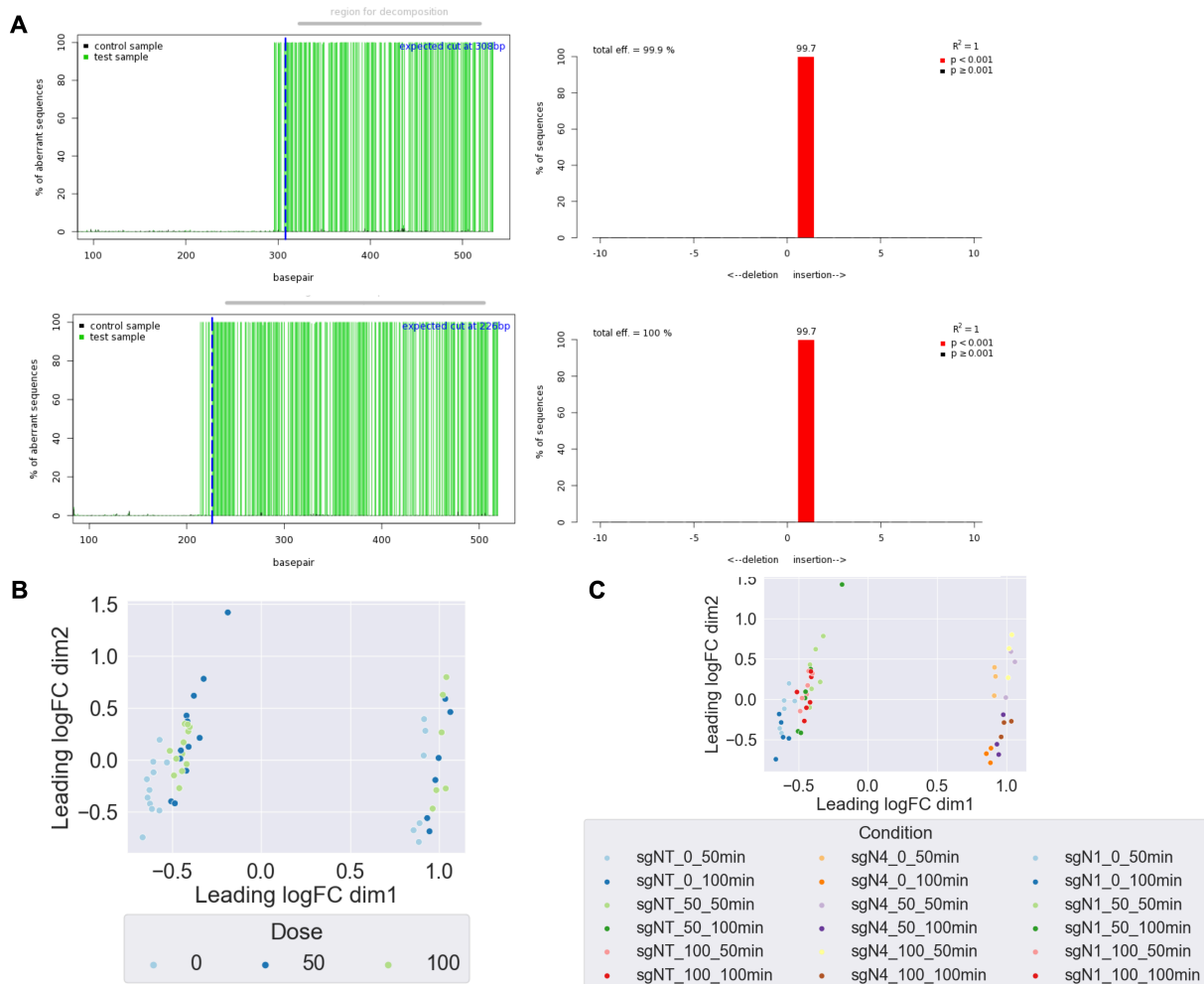
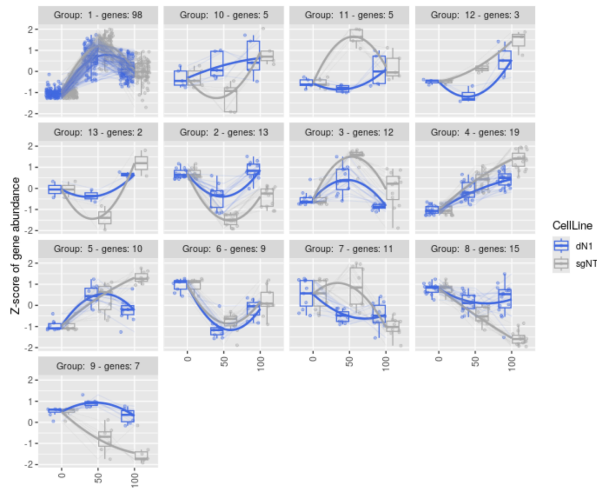


Figure 5.2. Supplementary Figure Related to Figure 2.2.

(A) Sequencing data of Δ NFAT1 (top) and Δ NFAT4 (bottom) clone gDNAs showing the % of aberrant sequences based on base pair (left), and the spectrum of indels around the cut site (right). (B) PCA plot of RNA-Seq data stratified by IgE antigen dose. (C) PCA plot of RNA-Seq data stratified by cell line, IgE antigen dose, and time point.

A Δ NFAT1 Low IgE



B Δ NFAT4 Low IgE

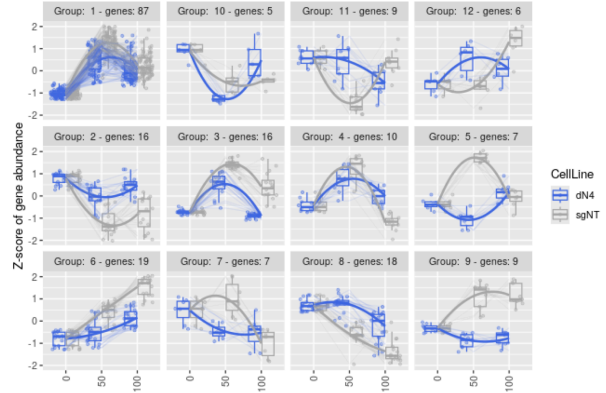


Figure 5.3. Supplementary Figure Related to Figure 2.3. (A) High IgE antigen responsive genes clustered by gene patterns in sgNT (grey) and dN1 (blue). sgNT = Non-Targeting sgRNA. dN1 = Δ NFAT1. (B) High IgE antigen responsive genes clustered by gene patterns in sgNT (grey) and dN4 (blue). sgNT = Non-Targeting sgRNA. dN4 = Δ NFAT4. (C) Characterization of gene clusters from A, represented as proportion of the total. (D) Characterization of gene clusters from B, represented as proportion of the total. (E) Representative genes from the clusters in A. (F) Representative genes from the clusters in B.

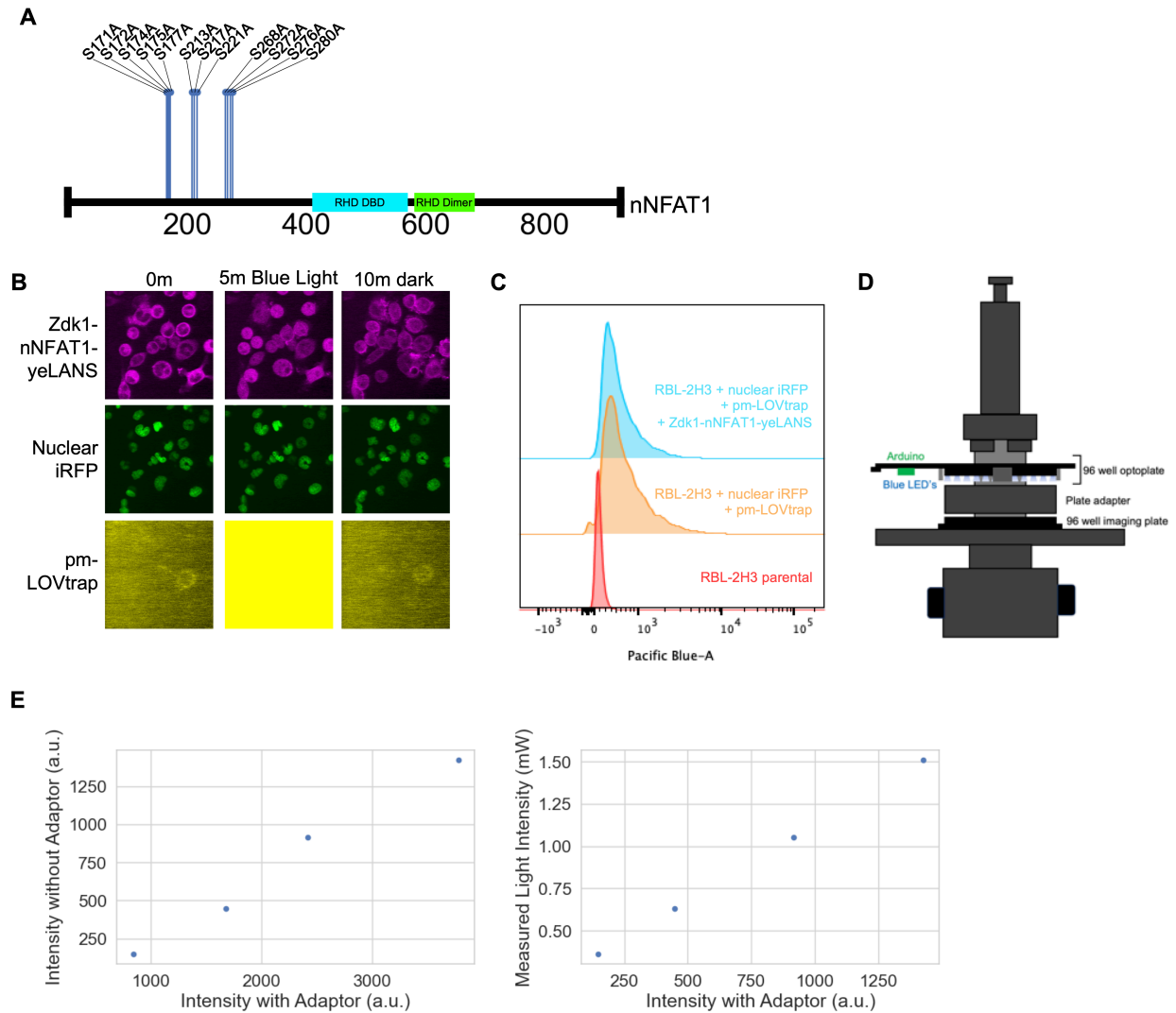


Figure 5.4. Supplementary Figure Related to Figure 2.4.

(A) Schematic of nNFAT1 constitutively nuclear mutations (See experimental methods “Modified NFAT1 (nNFAT1)”). (B) Images of nNFAT1-CLASP cells stimulated with 915 a.u. of blue light, showing Zdk1-nNFAT1-yeLANS (top), nuclear iRFP (middle), and pm-LOVtrap (bottom). (C) FACS data showing the expression of BFP (pm-LOVtrap) for nNFAT1-CLASP cells (top), trap only cells (middle) and parental RBL-2H3 cells (bottom). (D) Microscopy set up for blue light optoplate experiments. (E) Comparison of blue light intensity with and without the 96 well plate adaptor.

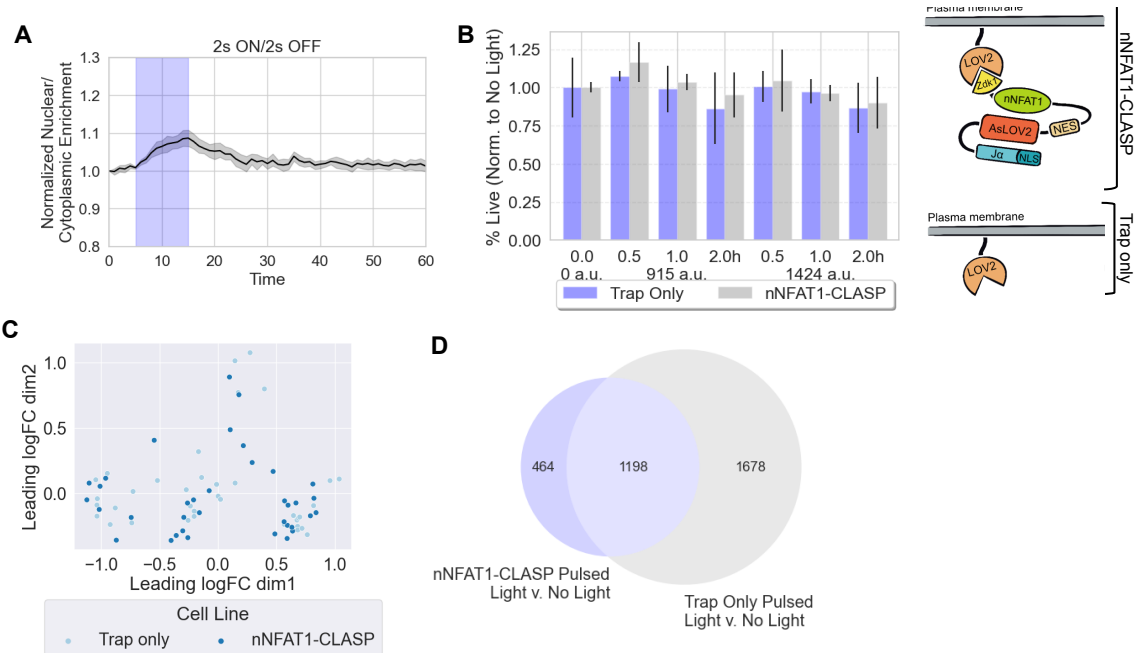


Figure 5.5. Supplementary Figure Related to Figure 2.5. (A) Normalized nuclear/cytoplasmic enrichment over time for nNFAT1-CLASP cells stimulated with 10 minutes of blue light in a pulsatile 2s ON/2s OFF regime. (B) Viability data showing the % of live cells, normalized to no light, for 0.5 to 2 hours of blue light in a 2s ON/2s OFF regime in nNFAT1-CLASP and Trap only cells. Schematic of nNFAT1-CLASP cells and Trap only cells is shown in the right panel. (C) PCA plot of RNA-Seq data stratified by cell line. (D) Venn diagram of the union of significantly differentially expressed genes in nNFAT1-CLASP cells and Trap only cells stimulated with pulsed light inputs.

CHAPTER 6. MATERIALS AND METHODS

Experimental details

Mammalian cell culture. RBL-2H3 cells were obtained from ATCC (CRL2256) and were cultured in DMEM (Fisher Scientific 10-569-044), 1% Antibiotic-Antimycotic (Thermo 15240062), and 10% Fetal Bovine Serum (GE Healthcare, SH30071.03). Serum was heated at 56°C for 30 minutes to heat inactivate. Serum was cooled to room temperature after heating, before mixing media.

Plasmid and cell line construction. Hierarchical golden gate assembly was used to assemble all plasmids (Table 6.1).^{17,18} BsaI and BsmBI sites were removed from parts to enable further assembly. Parts were generated through PCR or ordered as gBlocks from IDT. Plasmids were grown and prepared from DH5 α , XL1 Blue, Mach1, or Stbl3 competent cells (Macrolab, Berkeley, CA). For lentiviral transduction, plasmids were first transfected into LX293T cells at 80% confluency using Lipofectamine 2000 (Thermo 11668019), the plasmid of interest, and two plasmids encoding second generation lentiviral envelope and packaging vectors (MDG.2 and CMV). Transfection reagent and media were removed from LX293T cells approximately 16 hours later and transfected cells were re-fed with DMEM (Fisher Scientific 10-569-044), 1% Antibiotic-Antimycotic (Thermo 15240062), and 10% Fetal Bovine Serum. 24 hours later, the media was removed from transfected LX293T cells and filtered through a .45 micron filter to remove cell debris. Viral supernatant was then added to cells for transduction slowly on top of media. After addition of viral supernatant, cells were spun at 800xg for 45 minutes to increase transduction efficiency. After 24 hours of incubation with viral supernatant,

cells were re-fed with fresh media. After transduction, cells were sorted to select the population of interest.

Table 6.1 Plasmids

pSRT129	Nuclear iRFP	H2B iRFP670 UCOE
pSRT116	NFAT1-mScarlet	EF1ac-NFAT1 mScarlet
pSRT131	NFAT4-mScarlet	EF1ac-NFAT4 mScarlet
pSRT130	Trap	UCOE pCMV Lyn BFP asLOV2
pSRT054	NFAT1-CLASP	UCOE EF1ac Zdk NFAT1 yeLANS

Cell selection via sorting. To prepare for sorting, cells were lifted using trypsin and resuspended in the corresponding media to quench trypsin activity. Afterwards, cells were spun down at 400xg for 4 minutes to form a pellet. This pellet was then resuspended in PBS for sorting and placed on ice. Sorting was performed on a BD FACSAria II. BFP was assessed using the Pacific Blue channel (405 nm excitation, 450/50 nm filter), mScarlet was measured using the mCherry channel (561 nm excitation, 610/20 nm filter), and iRFP was assessed using the APC-Cy7 channel (633 nm excitation, 780/60 nm filter). Cells were sorted into fresh media and re-plated after sorting.

Modified NFAT1. Residues Ser¹⁷¹, Ser¹⁷², Ser¹⁷⁴, Ser¹⁷⁵, Ser¹⁷⁷, Ser²¹³, Ser²¹⁷, Ser²²¹, Ser²⁶⁸, Ser²⁷², Ser²⁷⁶, Ser²⁸⁰ in *H. Sapiens* NFAT1 (nfatc2) were mutated to alanines.

CRISPR clone generation. sgNT, ΔNFAT1, and ΔNFAT4 cell lines were generated using RNP editing. Guide RNA sequences targeting NFAT1 or NFAT4 were chosen from CRISPick (<https://portals.broadinstitute.org/gppx/crispick/public>) using the organism Rnor 6.0. Guide RNAs were assembled using 1:1 160uM tracrRNA (IDT 1072533) and

160uM crRNA (IDT Alt-R CRISPR-Cas9 crRNA, 10 nmol), for a final gRNA concentration of 80uM. gRNAs were incubated at 37C for 30 minutes (Table 6.2). Next, 1:1 of 40uM recombinant Cas9 (Macrolab, Berkeley, CA) was added to 80uM gRNA for a final RNP concentration of 20uM. RNP was incubated at 37C for 15 minutes. 1uL of HDR template (100 pmol HDRT) was added to each indexed well. Next, 5uL of RNPs were added to indexed wells of a 96-well polypropylene v-bottom plate for a final amount of 100 pmol RNP. Cells were lifted with trypsin and 1e5 cells per well were transferred to a centrifuge tube. Cells were spun at 90g for 8 minutes, and supernatant was aspirated with a vacuum. Cells were electroporated using the SF Cell Line 4D Kit S (Lonza V4XC-2023) protocol, with 20uL of cells per well. The surveyor assay was used to assess editing in the bulk populations, and to choose the guide RNA with the highest editing efficiency (T7 endonuclease I, New England Biolabs M0302L). Next, cells were single cell sorted in 96 well plate format to grow clonal populations. Cells were refed every 3 days and replated every 7 days. gDNA from clonal populations was extracted and the surveyor assay was performed (using 50% parental gDNA) to choose the highest efficiency clones. gDNA from the top 3 clones was sent for NGS sequencing by Primordium. PCR products around the cut site were used to validate the knockout (Table 6.3).

Table 6.2 sgRNA sequences used for CRISPR Cas9 knockout

sgNT	GGTTCTTGACTACCGTAATT
sgNFAT1-1	CTAGCGGGGCTCAAGCAAAG
sgNFAT1-2	ATGGAGTGATCTCGATCCGA
sgNFAT4-1	ACTGCTGGGTTATGATAGGG
sgNFAT4-2	ACTGAAATGGAAACGGTGCA
HDRT	GCCACCTACGGCAAGCTGACCCTGAAGTTCATCTGCACCACCGGC AAGCTGCCCCGTGCCCTGGCCCACCCTCGTGACCACCCTGACGTA CGGCGTGCAAGTGCCTTCAGCCGCTACCCCGACCACATGA

Table 6.3 Primers for PCR products used to validate CRISPR Cas9 knockout

NFAT1 F	GAGCGGGATGCCGGACGGGG
NFAT1 R	AGCCATGCAACCCTCTCGCCAGT
NFAT4 F	GGCTGAGCCCCAGACCAGCCT
NFAT4 R	AGCATGAAAACTGATCAGCAGCCA

Microscopy. For microscopy, a 96-well glass-bottom plate (Thermo Fisher 164588) was used. Cells were seeded at 15,000 cells/well in DMEM (Fisher Scientific 10-569-044), 1% Antibiotic-Antimycotic (Thermo 15240062), 10% Fetal Bovine Serum (GE Healthcare, SH30071.03). For environmental stimuli imaging, 100mM HEPES (Fisher Scientific BP299100) was added to the culture medium. 16-24 hours later, cells were imaged. Microscopy for all figures was performed on an inverted Nikon Ti microscope equipped with a CSU-22 spinning disk confocal, EMCCD camera, and custom 4-line solid state laser launch. Imaging took place inside a cage incubator which maintained temperature and humidity throughout the experiment. Images were taken using a 40x/0.95 objective, and cells were illuminated with 405, 561, and 640 nm lasers. For any images where cells are induced with light on this microscope, cells were covered

with a BreatheEasy seal and a custom-printed Optoplate holder was mounted on top of the cells. The Optoplate was then placed on top of the holder to induce the cells.

Drug induction. Purified mouse IgE κ Isotype Control (“IgE-TNP”, Clone C38-2, BD Biosciences 557079) 0.5 mg/mL stock was diluted to 3 ng/ μ L in cell culture media and cells were incubated overnight. 12 hours later, media was replaced with cell culture media + 100mM of HEPES (Fisher Scientific BP299100). TNP-BSA (Fisher Scientific NC0351576) 1 mg/mL stock solution was diluted to 200ng/mL or 100ng/mL and added to cells at time 0 at half the volume of the media in the well for a final concentration of 100ng/mL (“High IgE”) or 50ng/mL (“Low IgE”).

Light induction using Optoplate-96. Optoplate-96 was programmed using the OptoConfig-96 program.¹⁹ Cells were induced with 30 minutes of constant light input (for imaging experiments) or a pulsed light input of 2 seconds ON/ 2 seconds OFF for RNA-Sequencing experiments.

Optoplate intensity calculation. Optoplate intensities were calculated in the center of the well using the Thor labs PM100D energy meter and Puc sensor S120C.

RNA-Seq. Cells were seeded in black 24 well plates (Ibidi #82406). For the environmental stimuli, cells were pretreated with IgE-TNP 8 hours after seeding. 12 hours after IgE-TNP pre-treatment, cells were stimulated with TNP-BSA as described in *Drug induction* (time 0) and harvested at 50 minutes and 100 minutes. For the optogenetic experiments, media was replaced with cell culture media + 100mM of HEPES, and a BreatheEasy seal (Sigma Z380059) was placed on the cell plate. Blue light was delivered with a pulsed light input of 2 seconds ON/2 seconds OFF in 4 regimes: 915a.u., 1424a.u., 1424a.u. 10 minutes ON/50 minutes OFF, and 1424a.u. 10

minutes ON/20 minutes OFF. Cells were harvested at 30 minutes, 1 hour, and 2 hours. Cells were lysed using 300uL of TRIzol. Cell lysates were stored at -80 and RNA was extracted using the Direct-zol-96 RNA kit (Zymo Research R2054). After extraction, RNA quality was assessed using the Agilent RNA or High Sensitivity RNA ScreenTape on the TapeStation. RNA samples were diluted using Nanodrop concentrations and libraries were prepared and sequenced using 3' Tag-RNA-Seq protocols at the UC-Davis DNA technologies core.

Viability assay. Cells were seeded in a 96-well plate (Falcon 353219) at 15k cells per well in cell culture media. A BreatheEasy seal (Sigma Z380059) was placed on the cell plate and blue light was delivered in pulsed light input (2 seconds ON/2 seconds OFF) in 4 regimes: 915a.u., 1424a.u., 1424a.u. 10 minutes ON/50 minutes OFF, and 1424a.u. 10 minutes ON/20 minutes OFF. Directly after stimulation 20uL of CellTiter 96AQ (Promega G3580) was added directly to cells and left at 37C with 5% CO₂ for 2 hours. Absorbance was read using a Tecan Spark 10M plate reader.

Cellular proliferation assay. The CellTrace CFSE Cell Proliferation Kit for flow cytometry (Thermo Scientific C34554) was used to measure cell proliferation. Flow cytometry data was measured on an LSR Fortessa at 24h and 48h after addition of the CellTrace reagent. Samples were prepared for flow cytometry by removing media, rinsing with PBS, and trypsinized. Trypsin was quenched with cell culture media and cell suspensions were transferred to a 96-well round bottom plate (Fisher Scientific 08-772-2C). Cells were pelleted using centrifugation at 400xg for 4 minutes. Supernatant was removed and cell pellet was resuspended using 200uL of Flow buffer (PBS + 2% FBS). Cells were mixed prior to flow cytometry measurement.

Computational methods

Image analysis. Microscopy images are analyzed for nuclear and cytoplasmic intensity using a custom Python script modified from nuclealyzer, which depends on StarDist, Scikit-image, and OpenCV.^{20–22} First, images are resized to 60% of the original image to better match the StarDist training dataset. Next, StarDist is used on nuclear iRFP images to create masks of nuclei using the pretrained model '2D_paper_dsb2018'. Then, the cytoplasm is approximated by dilating the nuclear mask two times and subtracting a twice-eroded nuclear mask. Background of each image is estimated by choosing 100 random points throughout the image and taking the mean. Finally, OpenCV is used to track centroids of the nuclear masks throughout the experiment. Cells with a mean cytosol value calculated to be over 1.1 times the background, and cells where cytosol values were able to be calculated for over half the frames of the experiment, were kept. A baseline nuclear/cytoplasmic ratio is calculated by taking the average nuclear intensity/cytoplasmic intensity for the first two time points. Normalized nuclear/cytoplasmic enrichment is calculated as the average nuclear intensity/average cytoplasmic intensity at time T, divided by the baseline nuclear/cytoplasmic ratio.

Nuclear Import and Export Times. Individual cell traces were filtered by maximum normalized nuclear/cytoplasmic enrichment to only capture cells where nuclear translocation occurred. Cell data was smoothed using a Savgol filter from the SciPy library (Version 1.7.3).²³ Then, data was fit to $R(t) = R_0 + A*(1-\exp(-t/\tau_{in}))$ for nuclear import and $R(t) = R_0 + A*\exp(-t/\tau_{out})$ for nuclear export, where $R(t)$ is the normalized nuclear/cytoplasmic enrichment and R_0 is the normalized nuclear/cytoplasmic

enrichment at time 0. Data was fit only in the time range where nuclear import or export was occurring.

RNA-Seq. Differential expression analyses were conducted using limma-voom²⁴, limma version 3.58.1, edgeR version 4.0.9. DE analyses were conducted in R version 4.3.1 (2023-06-16)²⁵. The CRISPR model used in limma included cell line, a variable representing the waveform/timepoint combination used, and the interaction between cell line and waveform/timepoint. The CLASP model used in limma included cell line, a variable representing the waveform/timepoint combination used, and the interaction between cell line and waveform/timepoint. Genes were considered significant if the FDR corrected p-value was $< .05$. Network maps were generated using Enrichr.^{26–28} Gene ontology analysis was completed with the Molecular Signatures Database using hallmark gene sets (H), Reactome (C2), KEGG_LEGACY (C2), all transcription factor targets (TFT), GO biological process (C5), and GO molecular function (C5) for the species Rat.²⁹

CRISPR clone generation. NGS data of PCR products from CRISPR edited clones were analyzed using the TIDE tool.³⁰

Gene dynamics clustering. Genes from Figure 2.3 were clustered using the DEGpatterns function in the DEGreport package in R (Version 1.39.6), using the default settings and a $\text{minc} = 1$. Clusters were classified using the following criteria:

Unresponsive = Log_2FC difference between timepoint 50min or 100min and 0min < 0.6 .

Higher = Log_2FC difference between dN1 or dN4 and sgNT is ≥ 0.5 at 50min or

100min. Lower = Log_2FC difference between sgNT and dN1 or dN4 is ≥ 0.5 at 50min or 100min.

Data processing. Data processing was done with custom-written Python and R scripts, which are available upon request.

CHAPTER 7. REFERENCES

1. Huang W, Lin W, Chen B, et al. NFAT and NF- κ B dynamically co-regulate TCR and CAR signaling responses in human T cells. *Cell Reports*. 2023;42(7):112663.
doi:10.1016/j.celrep.2023.112663
2. Macian F. NFAT proteins: key regulators of T-cell development and function. *Nat Rev Immunol*. 2005;5(6):472-484. doi:10.1038/nri1632
3. Kar P, Parekh AB. Distinct spatial Ca²⁺ signatures selectively activate different NFAT transcription factor isoforms. *Mol Cell*. 2015;58(2):232-243.
doi:10.1016/j.molcel.2015.02.027
4. Mognol GP, Carneiro FRG, Robbs BK, Faget DV, Viola JPB. Cell cycle and apoptosis regulation by NFAT transcription factors: new roles for an old player. *Cell Death Dis*. 2016;7(4):e2199-e2199. doi:10.1038/cddis.2016.97
5. Martinez GJ, Pereira RM, Åijö T, et al. The transcription factor NFAT promotes exhaustion of activated CD8⁺ T cells. *Immunity*. 2015;42(2):265-278.
doi:10.1016/j.immuni.2015.01.006
6. Hannanta-anan P, Chow BY. Optogenetic Control of Calcium Oscillation Waveform Defines NFAT as an Integrator of Calcium Load. *Cell Systems*. 2016;2(4):283-288.
doi:10.1016/j.cels.2016.03.010
7. Yissachar N, Sharar Fischler T, Cohen AA, et al. Dynamic response diversity of NFAT isoforms in individual living cells. *Mol Cell*. 2013;49(2):322-330.
doi:10.1016/j.molcel.2012.11.003

8. Chen SY, Osimiri LC, Chevalier M, et al. Optogenetic Control Reveals Differential Promoter Interpretation of Transcription Factor Nuclear Translocation Dynamics. *Cell Systems*. 2020;11(4):336-353.e24. doi:10.1016/j.cels.2020.08.009
9. Osimiri LC, Bonny AR, Takagishi SR, et al. Optogenetic control of RelA reveals effect of transcription factor dynamics on downstream gene expression. Published online August 5, 2022:2022.08.03.502739. doi:10.1101/2022.08.03.502739
10. Antwi EB, Marrakchi Y, Çiçek Ö, Brox T, Di Ventura B. Requirements for mammalian promoters to decode transcription factor dynamics. *Nucleic Acids Research*. 2023;51(9):4674-4690. doi:10.1093/nar/gkad273
11. Turner H, Kinet JP. Signalling through the high-affinity IgE receptor FcεRI. *Nature*. 1999;402(6760):24-30. doi:10.1038/35037021
12. Theoharides TC, Alysandratos KD, Angelidou A, et al. Mast cells and inflammation. *Biochimica et Biophysica Acta (BBA) - Molecular Basis of Disease*. 2012;1822(1):21-33. doi:10.1016/j.bbadis.2010.12.014
13. Wang Q, Lepus CM, Raghu H, et al. IgE-mediated mast cell activation promotes inflammation and cartilage destruction in osteoarthritis. Kurosaki T, Taniguchi T, eds. *eLife*. 2019;8:e39905. doi:10.7554/eLife.39905
14. M.-G. Pan, Y. Xiong and F. Chen. NFAT Gene Family in Inflammation and Cancer. *Current Molecular Medicine*. 2013;13(4):543-554. doi:10.2174/1566524011313040007
15. Sharma M, Fu MP, Lu HY, et al. Human complete NFAT1 deficiency causes a triad of joint contractures, osteochondromas, and B-cell malignancy. *Blood*. 2022;140(17):1858-1874. doi:10.1182/blood.2022015674

16. Blue Light-Induced Gene Expression Alterations in Cultured Neurons Are the Result of Phototoxic Interactions with Neuronal Culture Media - PMC. Accessed April 13, 2024. <https://www.ncbi.nlm.nih.gov/pmc/articles/PMC6946540/>
17. A Toolkit for Rapid Modular Construction of Biological Circuits in Mammalian Cells | ACS Synthetic Biology. Accessed February 15, 2024. <https://pubs.acs.org/doi/10.1021/acssynbio.9b00322>
18. A Highly Characterized Yeast Toolkit for Modular, Multipart Assembly | ACS Synthetic Biology. Accessed February 15, 2024. <https://pubs.acs.org/doi/10.1021/sb500366v>
19. A graphical user interface to design high-throughput optogenetic experiments with the optoPlate-96 | Nature Protocols. Accessed February 15, 2024. <https://www.nature.com/articles/s41596-020-0349-x>
20. Weigert M, Schmidt U, Haase R, Sugawara K, Myers G. Star-convex Polyhedra for 3D Object Detection and Segmentation in Microscopy. In: *2020 IEEE Winter Conference on Applications of Computer Vision (WACV)*. ; 2020:3655-3662. doi:10.1109/WACV45572.2020.9093435
21. Schmidt U, Weigert M, Broaddus C, Myers G. Cell Detection with Star-Convex Polygons. In: Frangi AF, Schnabel JA, Davatzikos C, Alberola-López C, Fichtinger G, eds. *Medical Image Computing and Computer Assisted Intervention – MICCAI 2018*. Springer International Publishing; 2018:265-273. doi:10.1007/978-3-030-00934-2_30
22. Weinberg Z. *weinberz/nuclealyzer*: Public Release. Published online March 18, 2022. doi:10.5281/zenodo.6366817

23. SciPy 1.0: fundamental algorithms for scientific computing in Python | Nature Methods. Accessed March 30, 2024. <https://www.nature.com/articles/s41592-019-0686-2>
24. Ritchie ME, Phipson B, Wu D, et al. limma powers differential expression analyses for RNA-sequencing and microarray studies. *Nucleic Acids Research*. 2015;43(7):e47. doi:10.1093/nar/gkv007
25. R: The R Project for Statistical Computing. Accessed February 15, 2024. <https://www.r-project.org/>
26. Chen EY, Tan CM, Kou Y, et al. Enrichr: interactive and collaborative HTML5 gene list enrichment analysis tool. *BMC Bioinformatics*. 2013;14:128. doi:10.1186/1471-2105-14-128
27. Kuleshov MV, Jones MR, Rouillard AD, et al. Enrichr: a comprehensive gene set enrichment analysis web server 2016 update. *Nucleic Acids Res*. 2016;44(W1):W90-97. doi:10.1093/nar/gkw377
28. Gene Set Knowledge Discovery with Enrichr - Xie - 2021 - Current Protocols - Wiley Online Library. Accessed February 15, 2024. <https://currentprotocols.onlinelibrary.wiley.com/doi/10.1002/cpz1.90>
29. Subramanian A, Tamayo P, Mootha VK, et al. Gene set enrichment analysis: A knowledge-based approach for interpreting genome-wide expression profiles. *Proceedings of the National Academy of Sciences*. 2005;102(43):15545-15550. doi:10.1073/pnas.0506580102

30. Brinkman EK, Chen T, Amendola M, van Steensel B. Easy quantitative assessment of genome editing by sequence trace decomposition. *Nucleic Acids Research*. 2014;42(22):e168. doi:10.1093/nar/gku936

Publishing Agreement

It is the policy of the University to encourage open access and broad distribution of all theses, dissertations, and manuscripts. The Graduate Division will facilitate the distribution of UCSF theses, dissertations, and manuscripts to the UCSF Library for open access and distribution. UCSF will make such theses, dissertations, and manuscripts accessible to the public and will take reasonable steps to preserve these works in perpetuity.

I hereby grant the non-exclusive, perpetual right to The Regents of the University of California to reproduce, publicly display, distribute, preserve, and publish copies of my thesis, dissertation, or manuscript in any form or media, now existing or later derived, including access online for teaching, research, and public service purposes.

DocuSigned by:

9617DB5282CA420... Author Signature

4/18/2024

Date